Soft Matter

PAPER

Molecular dynamics study of nanoparticles and non-ionic surfactant at an oil–water interface†

R. J. K. Udayana Ranatunga,[a] **Chuong T. Nguyen,**[a] **Blake A. Wilson,**‡[a] **Wataru Shinoda**[b] **and Steven O. Nielsen*[a]**

Nanoparticles (NPs) and surfactants can spontaneously concentrate at the interface between two immiscible liquids, such as oil and water. Systems of high oil–water interfacial area, such as emulsions, are the basis of many industries and consumer products. Although NPs and surfactants are currently incorporated into many of these applications, their mutual interfacial behavior is not completely understood. Here we present molecular dynamics simulations of NPs and non-ionic surfactant in the vicinity of an oil–water interface. It was found that in low concentration the surfactants and NPs show cooperative behavior in lowering the oil–water interfacial tension, while at higher surfactant concentration this synergy is attenuated. It was also found that binding of surfactants to the NP surface decreases the surfactant efficiency in lowering the interfacial tension, while concurrently creating a barrier to NP aggregation.

1 Introduction

Surfactants, which are molecules containing both hydrophilic and hydrophobic segments, are prevalent in both nature and man-made products where they engage in an array of functions.[1] One of these functions is to lower the interfacial tension of two immiscible fluids in contact. Specifically, surfactants are driven by their amphiphilic nature to accumulate at oil–water interfaces and lower the oil–water interfacial tension. This property gives surfactants applications in the food, cosmetic, paint, polymer and oil industries.[2,3]

Distinct from surfactants, colloidal particles are also known to localize at fluid–fluid interfaces. Specifically, colloidal particles have been shown to strongly adsorb to oil–water interfaces, forming metastable oil and water emulsions. Such particle-stabilized emulsions are termed 'Pickering emulsions' after one of the pioneers in the field.[4] During recent years emphasis has been given to the localization of nanoscale colloidal particles (nanoparticles) at fluid–fluid interfaces, because of the possibility of creating novel materials through the unique properties shown by nanoparticle assemblies.[5–8]

Although both nanoparticles (NPs) and surfactants show affinity to bind to interfaces, the driving force for their localization stems from different roots. To understand this, consider a planar interface between two immiscible fluids, such as oil and water. The surface area of contact between oil and water, A_{ow}, is directly proportional to the excess free energy, G_{int}, associated with the oil–water interface: $G_{int} = \gamma_{ow}A_{ow}$, where γ_{ow}, the proportionality constant, is the oil–water interfacial tension. The excess interfacial free energy can be lowered by attacking either of the two factors involved, A_{ow} or γ_{ow}. This is essentially the difference between surfactants and NPs: surfactants lower γ_{ow} while NPs lower A_{ow}. As a consequence, systems comprised of both NPs and surfactants show complex and interesting behavior in the vicinity of a fluid–fluid interface. Investigating such physical behavior due solely to dispersive interactions is the aim of this article.

A majority of present day examples of nanoparticles and surfactants in co-existence are from applications where the surfactants are present as emulsifiers and the NPs are present in a capacity unrelated to their ability to modify surface energies. For example, nanoparticles can be used as pigments, antimicrobials, and ultraviolet absorbers. Such products include emulsion paints for house exteriors and vehicles,§ laundry and kitchen detergents,¶ and cosmetic and skincare emulsions.‖ Apart from these designed systems, the co-existence of

[a]*Department of Chemistry, University of Texas at Dallas, 800 West Campbell Road, Richardson, TX, 75080, USA. E-mail: steven.nielsen@ utdallas.edu; Fax: +1-(972)-883-2925; Tel: +1-(972)-883-5323*
[b]*Nanosystem Research Institute, National Institute of Advanced Industrial Science and Technology (AIST), 1-1-1 Umezono, Tsukuba, Ibaraki, 305-8568, Japan*

† Electronic Supplementary Information (ESI) available: Details on evaluation of the free energy profiles, calculation of the oil–water interfacial area removed by the nanoparticles and additional snapshots of systems are given. See DOI: 10.1039/c1sm05145h/
‡ Present address: Department of Chemistry, University of Texas at Tyler, 3900 University Blvd, Tyler, TX 75799, USA.

§ Behr® Process Corporation, DaimlerChrysler®, and Nanovations® produce emulsion paints containing nanoscale particles.
¶ Nanogist® offers products which claim to use antimicrobial silver nanoparticles of 1–10 nm size
‖ For example Applied Therapeutics® and Blue Lizard® offer skincare products which contain NPs

surfactants and NPs may sometimes be an unavoidable occurrence. For example, enhanced oil recovery relies on the floatation of oil aided by surfactants in environments containing naturally occurring NPs.[9]

When considering the wide range of systems which contain surfactants and NPs as constituents, it is clear that the physicochemical behavior of these systems warrants further investigation. Moreover, the rate at which new products are being introduced into the market and the safety concerns of products containing NPs imbue an urgency to understand these complex systems. Here we present molecular dynamics (MD) studies of uncharged NPs and non-ionic surfactant co-existing at an oil–water interface. Two main focuses are carried throughout this paper: first the effect that NPs and surfactants have on the interfacial tension of the oil–water interface, and second the synergy between NPs and surfactants.

Using MD is advantageous because of the precise control of simulation conditions allowed by the technique. This includes the preparation of chemically pure interfaces and exact control of component concentrations, both of which have a higher error experimentally. The spatial resolution of MD also allows for an examination of the components at a molecular scale and for direct calculation of thermodynamic quantities.

An appropriate illustration of the insight gained from using MD is the study of Luo et al.[9] Here, in contrast to our study which uses non-ionic surfactants, the investigators simulated systems of sodium dodecyl sulfate (SDS) surfactant and 1.2 nm sized hydrophobic NPs at trichloroethylene–water interfaces and found, among other things, that there is no cooperative action of surfactants and NPs at lowering the oil–water interfacial tension. Although this work exemplifies the use of computational studies to augment our conceptual understanding, it is clear that there is more work to be done and that our understanding of these complex systems is incomplete.

We have organized our paper in the following manner. In the methodology section details on the chosen system components and the MD force field are given. A list of simulations and details of analysis techniques are also given. In the results and discussion section, we first investigate the behavior of surfactants and NPs separately when localized at an oil–water interface. This includes the efficiency of our chosen surfactant, tri-(ethyleneglycol)-dodecyl ether, in lowering the oil–water interfacial tension, and also the adsorption of NPs at the oil–water interface. Next we investigate systems where these components are in the presence of one another, and study the system at different compositions. Afterwards, we study the effect of applying a Morse interaction potential, as opposed to a purely dispersive interaction, between the surfactants and the NP surface to mimic chemisorption. Emphasis is placed on the effect of this interaction on γ_{ow}. In the final section the effect of chemisorption on NP self-organization is reported.

2 Methodology

2.1 System components and force field

The MD technique requires a user specified force field which defines how the molecules are represented and specifies the interactions between them. To study systems of surfactants and NPs localized at an oil–water interface, four essential components are needed. The soft components, namely the surfactant, oil and water, are represented using the force field of Shinoda et al.[10] This force field has been parameterized according to experimental and atomistic MD data, and accurately predicts the oil–water interfacial tension and the phase behavior of surfactants.[10] Here, a coarse grained (CG) approach is adopted whereby three heavy atoms are grouped into one isotropic interaction site. There are many advantages of this approach in simulation studies aimed at understanding trends. CG representations often aid in understanding the physics of molecular systems by simplifying the dynamics of the system components while retaining a molecular viewpoint.[11] In accordance with this force field heptane, which is chosen as the oil phase, is represented with three CG beads. Three molecules of water are represented with a single CG water bead. The surfactant used in this study is the non-ionic amphiphile tri-(ethyleneglycol)-dodecyl ether, represented by a linear eight bead chain. In this force field the non-bonded interactions of uncharged beads are modeled through a Lennard-Jones function, which includes an attractive (dispersive) term as well as a repulsive (Pauli exclusion) term. Bonds and bends are treated through simple harmonic potentials. We refer any interested reader to the primary reference for further details.[10]

The sole hard component in this study is the NP, which is also represented using a kind of coarse grained model. Specifically, a mean field continuum approximation is made for the NP,[12] where a uniform distribution of interaction site density and a solid spherical geometry are assumed. The total interaction potential between the NP and another entity is simply the contribution of the interaction with each unit volume of the sphere summed over the entire NP, much like the Hamaker summation method.[13] Specifically, the potential energy between an interaction site within the NP and either a soft matter atom or an interaction site within another NP, separated by a distance d_{ij}, is taken as $U_{ij} = 4\varepsilon\left\{(\sigma/d_{ij})^{12} - (\sigma/d_{ij})^6\right\}$. Subsequently, the total interaction between the NP and a soft matter atom can be found through,

$$U_{np-i}(r; R) = \int_0^R a^2 da \int_0^{2\pi} d\theta \int_0^{\pi} \sin\phi \rho U_{ij}(d) \qquad (1)$$

where r is the distance between the center of mass of the NP and the soft matter atom, and ρ is the site density within the NP. The radius of the NP, R, enters eqn (1) through the integration limits. The integral can be evaluated analytically as shown in the supplementary information. The σ and ε parameters for the site-site interactions are generated using the Lorentz–Berthelot combining rules with the soft matter atom parameters taken from the CHARMM27 atomistic force field,[14] and $\varepsilon = 0.07$ kcal mol^{-1}, $\sigma = 3.55$ Å for the interaction sites within the NP. A site density value of $\rho = 0.113$ Å^{-3} was used for the solid NP. Since a coarse grained representation is used for the soft matter components an additional step is needed to map the interaction potential of a group of atoms to the corresponding CG potential, which was described in our previous work.[12] A nanoparticle radius of $R = 10.0$ Å was chosen for this study. The size and the interaction parameters result in a slightly hydrophobic NP (see Fig. 4), the characterization of which we discuss in subsequent sections.

The NP–NP potential energy is treated analogously through a six-dimensional integration over the site-site interactions.[15] The details are provided in the supplementary information and the resulting potential between two NPs in vacuum is shown as the dashed curve in Fig. 5.

To model covalent interactions between the NP and a ligand we use one of two functional forms. A non-dissociable bond between the NP and a ligand is modeled through a simple harmonic potential, namely,

$$U_h(r) = k(r - r_e)^2$$

where r is the separation between the attached ligand bead and the NP surface, and r_e the equilibrium separation, taken 3.00 Å away from the surface of the NP (to account for excluded volume).[12] Throughout the study k, the force constant of the bond, is taken as 100 kcal mol^{-1} Å^{-2}. Otherwise, in cases where we wish to study chemisorption of the soft components to the NP a Morse potential is used,

$$U_m(r) = D_e(1 - e^{-\alpha(r - r_e)})^2 \qquad (2)$$

where D_e is the dissociation energy and α is related to the curvature of the potential at r_e through $k = 2D_e\alpha^2$, where k is the the force constant of the bond. During this study we used three values of D_e (0.0, 39.7, and 99.4 kcal mol^{-1}) to represent different binding energies.** Note that our modeling choice results in the ligands being mobile on the NP surface; for an experimental realization of this phenomenon see Jackson et al.[16]

2.2 Composition of simulation systems

Molecular dynamics simulations were run using the MPDyn package[17] under isothermal-isobaric conditions (NPT), using a Nosé-Hoover thermostat[18] at a temperature of 300.15 K, and an Andersen barostat[19] at a pressure of 0.1 MPa, respectively. The multistep rRESPA[20] algorithm was used with a timestep of 20 fs for long ranged non-bonded interactions, and a 2 fs time-step for short-ranged non-bonded and all bonded interactions. Periodic boundary conditions were enforced in all three directions.

All the systems include the two solvents, water and heptane, which were initially separated into two blocks such that the oil–water interface is perpendicular to the z axis. Under the NPT ensemble, the system evolves to minimize the Gibbs free energy and hence to minimize the oil–water interfacial area. This tends to maintain a planar interface between oil and water while also shrinking the unit cell in the x and y directions. Hence, to prevent the simulation unit cell from thinning in the x–y direction the barostat is allowed to act only in the z direction.

The setup described above is representative of oil–water systems of negligible curvature on the nanometre length scale. For example an emulsion droplet of radius 400 nm would correspond to an interfacial curvature of less than ±1 Å across a 125 Å wide simulation box. The presence of a planar interface

also allows for a straightforward calculation of the oil–water interfacial tension, γ_{ow}, from the virial expression,[21]

$$\gamma_{ow} = \frac{1}{2}\left\langle L_z\left(P_{zz} - \frac{P_{xx} + P_{yy}}{2}\right)\right\rangle$$

where L_i is the box length in the i = x/y/z direction, P is the system pressure tensor, and the oil–water interfacial tension γ_{ow} is defined as $\gamma_{ow} = (\partial G_{int}/\partial A_{ow})_{NPT}$. Here G_{int} is the interfacial excess free energy and A_{ow} is the apparent oil–water interfacial area, which is simply $L_x \times L_y$ for a pure oil–water interface. The apparent interfacial area, which is often used in experiments,[22] ignores undulations of the interface due to capillary waves and buckling due to tensionless interfaces, etc. It should also be noted that the above equation represents the interfacial tension of the two interfaces with a single value, implying two equivalent interfaces in the system.†† Although this is not strictly true in some cases this does not detract from the qualitative importance of γ_{ow} since it represents the average value.

A representative side-view of a simulation box is given in the left panel of Fig. 1. The right panel shows the time averaged mass density plots of each component as a function of the z coordinate. As shown in the snapshot there are two oil–water interfaces in each simulation box due to the use of periodic boundary conditions. The average positions of these interfaces are taken as the crossing points of the water and heptane mass densities. The surfactant and NP density profiles show peaks overlapping the fluid interfaces characteristic of interfacial localization.
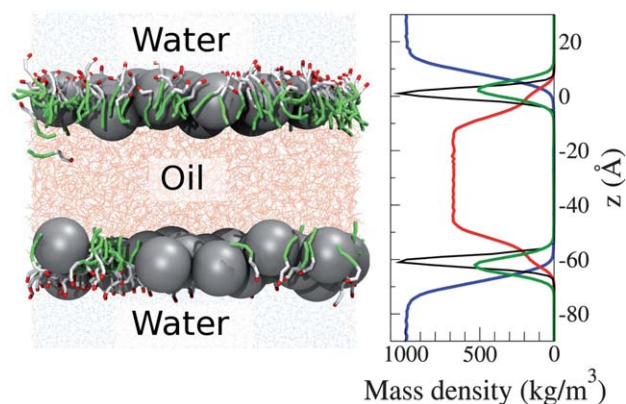

Fig. 1 Simulation setup. (*left panel*) Side view of a representative simulation box showing the heptane slab and water slab. The NPs and surfactants localize at the two oil–water interfaces. The alkane segment of the surfactant has been colored green. (*right panel*) Mass density profiles of the system components. The profile of heptane is shown in red (the middle solvent block in the side view), the water in blue and surfactant in green. The density profile of the NPs (shown in black) has been divided by a factor of two to bring all the profiles to a comparable scale.

** To put this range of dissociation energies in context, gold–thiol bonds are reported in the range 30–40 kcal mol^{-1}, while carbon-carbon single bonds are in the range 80–85 kcal mol^{-1}.

†† For series (E), which has one pure oil–water interface and one interface with surfactant functionalized NPs, this equation has to be modified. In this case the equation is not divided by two but instead γ_{ow} of the pure oil–water interface (which we have previously determined) is subtracted to yield the interfacial tension of the interface containing NPs.

Throughout this study, the systems were equilibrated for 10 ns prior to data collection runs of at least 10 ns. The initial coordinates of the system were chosen such that all NPs and surfactants were either distributed equally among the two interfaces (series A–D) or were localized at only one interface (series E). Depending on their concentration, NPs and surfactants may desorb from the interface into the heptane phase during the simulation. This is expected for tri-(ethyleneglycol)-dodecyl ether surfactant considering the solubility of polyethylene glycol (PEG) chains in alkane solvent. Care was taken to sample from trajectories after establishment of dynamic equilibrium of all components partitioning between the oil–water interface and the solvent phases. To confirm equilibrium, mass density plots averaged over 1 ns intervals were calculated and are shown in Fig. 2 for a representative simulation. The overlap of the profiles clearly shows that there is no net mass transfer with time. The convergence of interfacial tension measurements with time also corroborate that all the systems studied reached equilibrium within 10 ns.

Five series of simulations were carried out (see Table 1), all of which contain oil–water interfaces. The numbers of surfactants and NPs given in Table 1 are for those initially located at each interface while the (x2) is used to indicate that there are two such interfaces in the system. The first series (denoted series A) comprises simulations where only surfactant is present and no NPs are involved. In the second series (series B) both NPs and surfactants are present, and both their concentrations are varied. In the third series (series C) the concentration of surfactant is fixed while the concentration of the NP is varied. Series (A), (B), and (C) all represent systems where there is no covalent bonding between the surfactant and the NP. In the fourth series (series D), the effect of including covalent binding between the NP and the surfactant is investigated. This is accomplished by assigning a Morse potential between the NP and the alkane termini of the surfactant. In this series only a single NP is used. In series (E) all surfactants are irreversibly tethered to the NP surface through
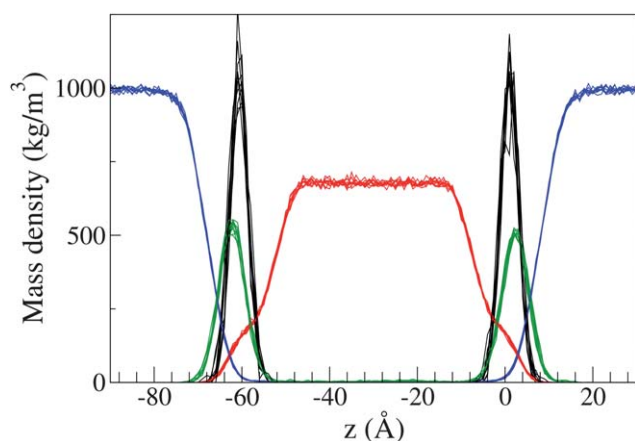
Table 1 Summary of simulations

Label	NPs	$C_{12}E_3$	Box Dimensions (Å)	Duration (ns)
A1	0	0×2	$125 \times 125 \times 124$	10/10
A2	0	120×2	$125 \times 125 \times 113$	10/10
A3	0	240×2	$125 \times 125 \times 112$	10/10
A4	0	360×2	$125 \times 125 \times 116$	10/10
A5	0	480×2	$125 \times 125 \times 122$	10/10
B1	24×2	0×2	$125 \times 125 \times 132$	10/10
B2	18×2	120×2	$125 \times 125 \times 129$	10/10
B3	12×2	240×2	$125 \times 125 \times 128$	10/10
B4	6×2	360×2	$125 \times 125 \times 129$	10/10
B5	0×2	480×2	$125 \times 125 \times 131$	10/10
C1	24×2	240×2	$125 \times 125 \times 158$	10/50
C2	18×2	240×2	$125 \times 125 \times 153$	10/50
C3	12×2	240×2	$125 \times 125 \times 147$	10/50
C4	0×2	240×2	$125 \times 125 \times 142$	10/50
D1[a]	1×2	0×2	$100 \times 100 \times 174$	10/10
D2[a]	1×2	50×2	$100 \times 100 \times 172$	10/10
D3[a]	1×2	100×2	$100 \times 100 \times 171$	10/10
D4[a]	1×2	150×2	$100 \times 100 \times 174$	10/10
D5[a]	1×2	300×2	$100 \times 100 \times 183$	10/10
E1(B2)	18	126(7 ea)	$125 \times 125 \times 120$	10/10
E2(B3)	12	240(20 ea)	$125 \times 125 \times 132$	10/10
E3(B4)	6	360(60 ea)	$125 \times 125 \times 113$	10/10
E4(C1)	24	240(10 ea)	$125 \times 125 \times 153$	10/10
E5(C2)	18	252(14 ea)	$125 \times 125 \times 147$	10/10
E6(C3)	12	240(20 ea)	$125 \times 125 \times 131$	10/10

[a] Simulations were repeated for varying NP–surfactant Morse bond energies of $D_e = 0.0$, 39.7, and 99.4 kcal mol^{-1}.

a harmonic potential. This series used similar concentrations of NPs and surfactants as those of series (B) and (C) (as indicated in Table 1), and examines the changes in the system behavior when the surfactants are surface ligated to the NPs. For series (E) only one oil–water interface was populated with surfactant functionalized NPs and the numbers in parentheses in the third column of Table 1 are the number of surfactants per NP.

3 Results and discussion

3.1 Interfacial behavior of simulated NPs and surfactants

We first discuss the separate behavior of NPs and surfactants at an oil–water interface prior to discussing their concerted behavior. This builds a strong foundation and a context to examine more complex systems.

3.2 Surfactant interfacial behavior

In this study we focus on tri-(ethyleneglycol)-dodecyl ether surfactant. We have chosen a non-ionic surfactant because these create robust dispersions, insensitive to environmental variables such as pH and ionic strength.[23] The use of a non-ionic system also provides insight into the relationship between the dispersive interactions among species and the overall behavior of the system. This is powerful because of the ubiquity of dispersion interactions in all chemical systems. This approach also avoids the complications of electrostatic adsorption of surfactants to the surface of NPs which is thought to be a significant factor in many experimental[24,25] and computational studies.[9]

Fig. 2 Profiles of mass density as a function of z position. The profile of each component is plotted in 1 ns time-averaged blocks for simulations from 10 ns–20 ns from the initial configuration. The overlap of the profiles indicates that there is no net movement of components and hence that the system has reached equilibrium. The mass density of the NPs has been divided by a factor of two, and the color scheme is consistent with Fig. 1.

From a number of non-ionic surfactants available to study, the class of PEG-alkane surfactants are significant because of their biocompatibility, solubility and chemical inertness.[26] The linear PEG-alkane surfactants are particularly good candidates for a generic study because of their efficiency and effectivity at lowering the oil–water interfacial tension. These surfactants have a block copolymer topology given by $HO(CH_2CH_2O)_x(CH_2)_{y-1}CH_3$ where x represents the number of ethylene glycol units and y represents the number of carbons in the alkane block, respectively. The tri-(ethyleneglycol)-dodecyl ether surfactant used for our studies is denoted as $C_{12}E_3$, where x = 3 and y = 12. This surfactant is considered to have an extended as opposed to a compact head group.[27]

3.2.0.1 Series (A). To characterize the interfacial activity of $C_{12}E_3$ at oil–water interfaces, a series of simulations (series A) was carried out by varying the concentration of the surfactant. $C_{12}E_3$ spontaneously localized at the oil–water interface and created a Gibbs monolayer, with slight solubility in the heptane (oil) phase. The effect of the surfactant on the oil–water interfacial tension, γ_{ow}, is assessed using the virial expression described in the methods section. The plot of γ_{ow} as a function of nominal interfacial area per surfactant is shown in Fig. 3. Here, the nominal interfacial coverage is simply the initial surfactant number at the oil–water interface divided by the apparent interfacial area.

The pure heptane/water interface shows an interfacial tension of ~50.1 mN m^{-1},‡‡ which can be thought of as γ_{ow} at infinite dilution of surfactant. With increasing $C_{12}E_3$ surface concentration, γ_{ow} is progressively lowered to a tensionless state at $C_{12}E_3$ coverages of ~32 Å^2 per surfactant. It should be emphasized that the abscissa of Fig. 3 is the nominal interfacial concentration although the solubility of the surfactant in oil causes some surfactant to be desorbed from the interface (see ESI†).

3.3 Nanoparticle interfacial behavior

In contrast to surfactants, particles are driven to oil–water interfaces to remove contact between the two liquids. Consider a single nanoparticle p of radius R in the vicinity of an oil–water interface. Depending on its position the particle shares interfaces with oil and water, with surface tensions γ_{po} and γ_{pw}, respectively. Each of these interfaces contributes to the free energy of the system, allowing for a simple formulation of the total interfacial excess free energy.

$$G_{int} = A_{ow}\gamma_{ow} + A_{po}\gamma_{po} + A_{pw}\gamma_{pw} \quad (3)$$

where A_{ij} represents the surface area of each interface. Assuming a spherical particle geometry, the change in free energy due to varying the particle position can be given explicitly, from a free energy reference state of the particle completely immersed in the oil phase.

$$G(\eta) = -\pi(R^2 - \eta^2)\gamma_{ow} + 2\pi R^2\{(1 + \eta/R)(\gamma_{pw} - \gamma_{po})\} \quad (4)$$

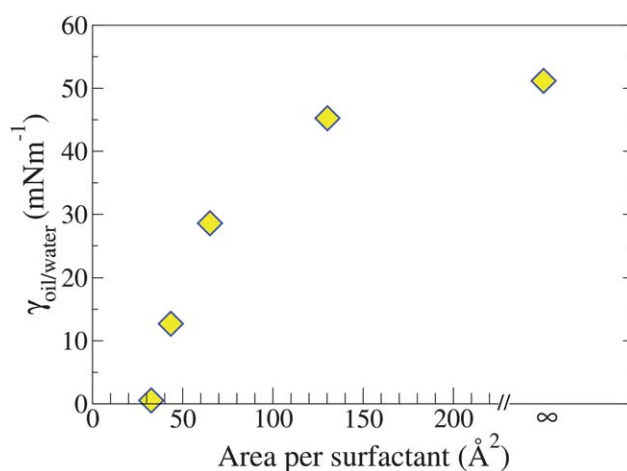‡‡ The interfacial tension for many alkane/water systems is of similar magnitude

Fig. 3 Oil–water interfacial tension (γ_{ow}) data from series (A), where $C_{12}E_3$ surfactant localized at the interface acts to lower γ_{ow}.

where the variable η is the distance of the NP center from the interface, and the profile is defined for the region $-R < \eta < R$.[28] The first term of this equation is a stabilization of the system due to removal of oil–water contact, which is the driving force for particle localization at the interface. From minimizing eqn (4) with respect to the particle position, η, we can obtain the equilibrium particle position η_0 corresponding to the lowest free energy. This is Young's equation, where the contact angle, θ, is an experimental observable.

$$\frac{\eta_0}{R} = \cos\theta = \frac{\gamma_{po} - \gamma_{pw}}{\gamma_{ow}} \quad (5)$$

Young's equation, and modifications to make it more accurate,[29] imbues the contact angle with the status of a thermodynamic property which is independent of the NP concentration. On the other hand the Gibbs adsorption equation shows unequivocally (for a liquid–vapor system) that localization of any solute at an interface results in a lowering of the surface tension,[30,31] which would indicate dependance of the contact angle on the concentration of adsorbed particles, specifically through the γ_{ow} term in eqn (5). However, what is observed experimentally is that NP localization at oil–water interfaces rarely lowers the surface tension appreciably.[24,32–34] This is also what we observed in the present study, namely that particle localization at the interface does not result in a lowering of γ_{ow}.

3.3.0.2 Transfer free energy profile. Using constrained molecular dynamics (CMD)[29] the oil to water transfer free energy profile of a single 10.0 Å radius NP was determined as shown in Fig. 4.

The NP has a free energy minimum at the interface, with an equilibrium position $\eta_0 \sim -1.3$ Å and an interfacial binding energy of 26 kcal mol^{-1}. This binding energy value is appreciable higher than the ambient thermal energy which suggests that the particle will not spontaneously desorb from a pure oil–water interface. The particle prefers solvation in the heptane phase with a transfer free energy of 27 kcal mol^{-1}; any desorption event will thus likely be into the heptane phase.
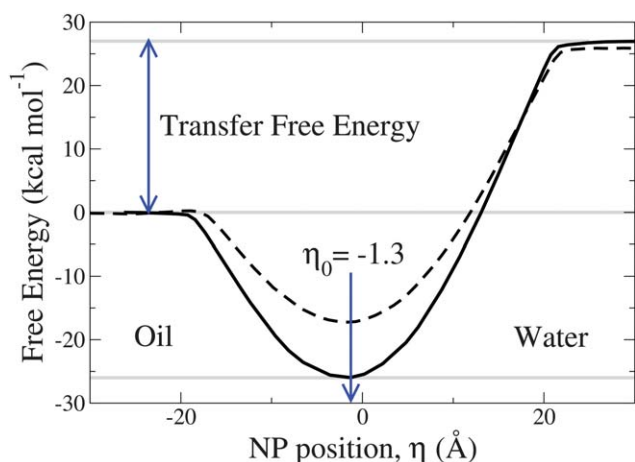
Fig. 4 The oil to water transfer free energy profile for a 10.0 Å radius NP. The solid line is for a pure oil–water interface. The dashed curve is for an oil–water interface with a nominal $C_{12}E_3$ interfacial concentration of 100 Å² per surfactant.

The features of the profile shown in Fig. 4 follow the predictions of eqn (4). The interfacial binding free energy depends on the oil–water interfacial tension, γ_{ow}, and thus may be modified by adding surfactants to the system. This is illustrated in Fig. 4 for a nominal interfacial coverage of 100 Å² per surfactant. This surfactant coverage corresponds to an interfacial tension of ~39 mN m⁻¹ (see Fig. 3). This lower γ_{ow} value results in a decrease in the NP interfacial binding free energy which will be important later.

In general the magnitude of the binding free energy is also strongly dependent on the size of the NP. As noted by Lin *et al.*,[35] and in accordance with eqn (4), the binding free energy scales as the square of the NP radius and therefore larger particles are more strongly adsorbed to the interface.

Fig. 4 only shows the oil to water transfer free energy of an individual NP. The transfer free energy profile in the presence of other NPs is expected to be more complex due to particle–particle interactions. Although a detailed analysis is beyond the scope of our study, the role that interactions between NPs play in their behavior at interfaces cannot be overlooked, and in the following section we study the interaction between two NPs at an oil–water interface.

3.3.0.3 Dimerization free energy profile. The NP modeled in this study is uncharged, hence the interaction between two NPs is purely dispersive in character. The NP–NP interaction potential energy, shown in Fig. 5, reaches its minimum at the interparticle contact separation of ~22.1 Å.

The NP dimerization free energy profile, for two NPs localized at an oil–water interface, indirectly involves the solvent-particle interactions which can impart a different form to the free energy as compared to the NP–NP potential energy. The free energy profile for two 10.0 Å radius NPs is given in Fig. 5. Due to solvent layering the free energy profile takes an oscillatory form. The free energy minimum at particle–particle contact is −2.7 kcal mol⁻¹ which implies that thermally driven dissociation is infrequent. The secondary minimum at ~27 Å is commensurate with the thickness of a solvent layer. However, this thickness is
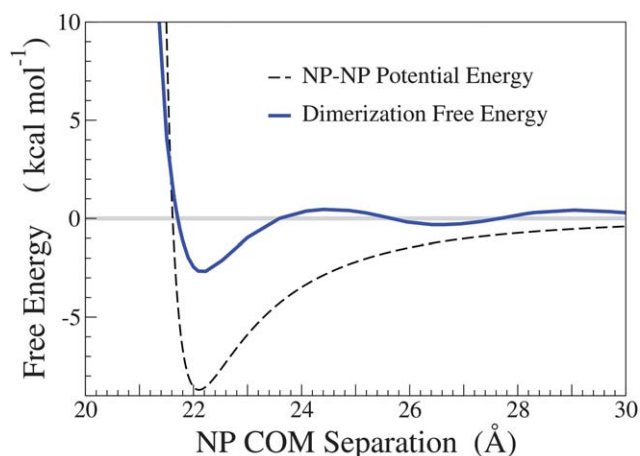

Fig. 5 Potential energy between two 10.0 Å radius NPs as a function of their center of mass (COM) separation (dashed line), and their dimerization free energy profile at an oil–water interface (solid line). The first minimum is when the particles are in contact with one another and the oscillations in the profile are due to solvent layering.

dependent on the model used, hence we would expect a smaller oscillation wavelength for a smaller solvent bead. The features observed in the dimerization free energy profile are seen more generally in systems containing many particles, where the particles are seen to aggregate at the oil–water interface. An example of this aggregation behavior is shown in Fig. 6.

3.4 Mutual interfacial behavior of NPs and surfactants

In this section we examine the effect that NPs and surfactants have on one another. Let us define two reference states, the first for an oil–water system with only surfactant localized at the interface, and the second with only NPs localized at the interface. The first reference state was chosen at the surfactant concentration needed to reduce the oil–water interfacial tension to zero. From series (A) this was found to be at 32.55 Å² per surfactant, which corresponds to 480 surfactants for an apparent interfacial
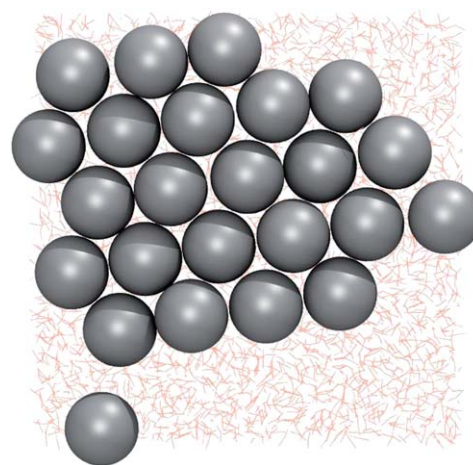

Fig. 6 The aggregation of NPs at the oil–water interface. The image shows a top-down view of a representative snapshot of system (B1) at equilibrium.

area of 125×125 Å^2. For the second reference state, with only NPs localized at the interface, a system composition was chosen with 24 NPs for the same apparent surface area (125×125 Å^2). Using these reference states as upper bounds simulation series (B) and (C) were designed.

3.4.0.4 Series (B). Table 1 gives the composition of the systems simulated under series (B) where the numbers of both NPs and surfactants were varied linearly from the reference states to zero over five points. It should be noted that the number of surfactants for this series is essentially the same as for series (A), while the number of NPs varies from 0 to 24. The simulation box sizes were also kept similar for ease of comparison.

The apparent interfacial coverage *versus* the surface tension for series (B) is plotted in Fig. 7, along with series (A). The far right points of the plot are at zero surfactant coverage, where (A1) represents a pure oil–water interface while (B1) comprises 24 NPs at an oil–water interface (shown in Fig. 6). As stated previously the interfacial tension of (B1) does not change significantly from that of a pure oil–water interface. As the surfactant concentration is increased (B1 → B5, or going from right to left in Fig. 7), the interfacial tension is lowered for both series, but for the same area per surfactant series (B) shows lower interfacial tensions. At the leftmost points in Fig. 7, the two series are equivalent and as expected give nearly tensionless states.

Comparison of the surface tensions for the intermediate points of series (A) and (B) in Fig. 7 clearly shows that the presence of NPs makes the surfactant more efficient at lowering γ_{ow}.

The synergy of surfactants and particles in stabilizing oil–water emulsions has been observed experimentally.[24] For example Tambe and Sharma found that addition of steric acid increased the stability of oil/brine emulsions stabilized with inorganic particles,[36] and Wang *et al.* found that addition of dodecyl amine surfactant aided in stabilization of petroleum emulsions through kaolinite particles.[37] In both these cases the synergy was attributed to the ability of surfactants to adsorb to the surface of the particles and hence modify their contact angle.
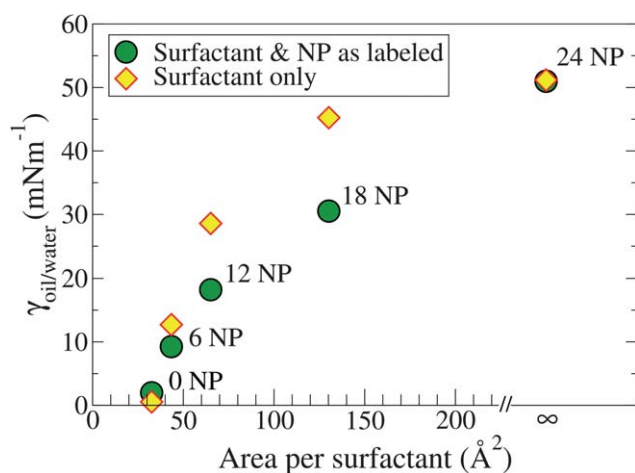
Moreover, several studies of charged particles with non-ionic surfactant show that this pairing is synergetic in stabilizing emulsions,[38–40] although some of this synergy is attributed to flocculation of the particles. Generally, it is found that the synergy exists at low surfactant concentration, whereas at higher concentration the particles and surfactants compete for 'adsorption sites' at the interface.

In this study we have chosen a non-ionic species, therefore electrostatic charge driven adsorption of surfactant onto particles does not occur. In addition the modeled NPs are not surface active (in the sense of lowering γ_{ow}), hence this system provides a unique opportunity to extract information about the behavior of NPs and surfactants through γ_{ow} measurements.

Returning to Fig. 7, the differences in surface tension are most pronounced for systems (A2) and (B2), namely with 18 NPs localized at the interface. The difference in surface tension decreases on either side of this point, which can be expected. At lower area per surfactant, the number of NPs is low in series (B), limiting the extent of any synergistic effect. Towards the other end of the plot the surfactant coverage is too low to substantially lower the interfacial tension.

The most straightforward explanation of the synergy of NPs and surfactants in lowering γ_{ow} is the excluded volume of interfacially localized NPs. For a fixed box size, NPs reduce the actual area of contact between oil and water by localizing at interfacial positions. For example consider system B2 which shows the highest synergy. The removal of interfacial area due to the NPs effectively reduces the oil–water contact area from 15,625 Å^2 to 9,160 Å^2§§ and hence the effective interfacial area per surfactant to 76 Å^2 from the value of 132 Å^2 when the NP excluded volume is not considered. Using the γ_{ow} values from series (A) we would predict an oil–water interfacial tension of 30–35 mN m^{-1} for this reduced coverage of surfactant which is the actual surface tension value observed for (B2).

3.4.0.5 Series (C). To further investigate systems of surfactants and NPs, simulation series (C) was carried out where the surfactant coverage was kept constant while the number of NPs was varied from 0 to 24 with a fixed interfacial area of 125×125 Å^2. The surfactant coverage is half of what is needed to lower γ_{ow} to zero. If the NPs remain localized at the interface, 24 of them would account for the remaining half of the interfacial area and one could expect a monotone decrease of γ_{ow} to zero as the number of NPs is increased from 0 to 24. The evidence from the transfer free energy profiles re-enforces this hypothesis. Eqn (4) states that the free energy of adsorption to the interface from the oil phase is parametrically dependent on γ_{ow}, and although the oil–water interfacial tension is lowered by the presence of surfactants at the interface, the free energy minimum is not completely removed. We could therefore expect localization of NPs at the oil–water interface to continue until the magnitude of the binding energy is surmountable through thermal fluctuations. However, the actual oil–water interfacial tension values, shown in Fig. 8, disprove this hypothesis.

Fig. 7 Comparison of γ_{ow} for series (A) and (B). Series (A) comprises surfactant only (previously shown in Fig. 3) while series (B) comprises NPs and surfactant at an oil–water interface.

§§ The ensemble averaged z position of the NPs can be used to calculate the area removed from the interface assuming a particle radius of 11.1 Å. Further details are given in the supplementary information.

The interfacial tension is lowered initially and then plateaus instead of dropping to zero. It is clear that after an initial lowering of γ_{ow} the free energy of the system is no longer dominated by the oil–water interface. Clues towards the behavior of the system can be found by inspection of the snapshots shown in Fig. 9.

Fig. 9 shows the onset of multi-layering of NPs with increased concentration. Two reasons are proposed for the observed desorption from the interface and the creation of a second layer below the interfacial NPs. The first is an appreciable interaction energy between two NPs in contact (see Fig. 5). The second, which is related, is that aggregation removes some particle-solvent contact area, $i.e.$ the contact of two particles which occurs in the oil phase lowers A_{po} in eqn (3). Neither of these factors are addressed in the transfer free energy profiles of the type shown in Fig. 4 which are for isolated particles. A more complete set of data would account for the concentration of particles in the system, and might show a lower free energy for particles in the oil phase due to particle–particle and other interactions. However, evaluation of these free energies is a complex problem and outside the scope of this study.

In this section we revealed the behavior of uncharged NPs and surfactants at oil–water interface. At low surfactant coverage, NPs adsorb strongly to the interface and lower the surface area that the surfactant has to protect. This leads to a synergy between NPs and surfactants in lowering the oil–water interfacial tension. At higher surfactant concentration the driving force for localization of NPs to the oil–water interface is diminished, and other factors such as the particle–particle interactions become important. In this sense there is an indirect competition between the surfactants and the NPs to bind to the oil–water interface. Under this competition, the synergy between NPs and surfactants becomes less important, and addition of either species to the system does not appreciably lower the oil–water interfacial tension.
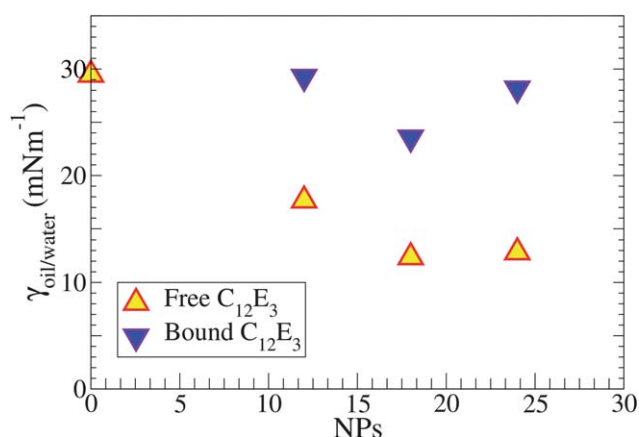
Given that we limit ourselves to studying a single size of NP it is pertinent to discuss the role of particle size on the synergy between particles and surfactant in lowering the oil–water interfacial tension. For a given mass of solid particles, smaller particles will be able to remove more oil–water interface. Therefore, according to the hypothesis we propose here, smaller particles will have a greater synergy with surfactant. However it could be expected that this is only true while the NPs are large enough to avoid thermal desorption from the interface. Furthermore, it is not obvious how the desorption of particles in states of low oil–water interfacial tensions will proceed because particle–particle interactions within the oil phase play a role in determining the particle behavior under these conditions. In general we can speculate that for other sizes of particles the same trends will be observed: synergy at lower concentrations of surfactant and NP, and competitive adsorption at higher concentrations, although their magnitude and onset would be difficult to predict.

3.5 Effect of covalent interactions between surfactants and NPs

In the previous sections the interaction between surfactants and NPs was modeled to be completely dispersive in nature, and the synergy in lowering the oil–water interfacial tension was through surfactant interfacial activity enhanced by NP exclusion of oil–water contact area. Often though, surfactants may chemisorb to NPs. Here we study surfactant/NP systems in the presence of such a covalent interaction, which we model with a Morse potential between the surfactant alkane terminus and the surface of the NP (eqn (2)).

3.5.0.6 Series (D). Simulations of individual NPs at oil–water interfaces were performed with different numbers of surfactants in the system. These simulations were then repeated by varying the bond energy between the NP and the hydrophobic terminus of the $C_{12}E_3$ surfactant. Fig. 10 contrasts the behavior of 100 $C_{12}E_3$ surfactants in the presence $versus$ absence of a Morse potential of dissociation energy $D_e = 39.7$ kcal mol^{-1}.

An increase in the number of surfactants adsorbed (bound) to the NP is seen as D_e is increased, until the surface of the NP is saturated with surfactant. The energy gained by the binding of surfactants onto the NP is countered by: (1) the entropic penalty of confining the surfactants onto the NP surface, (2) the energy penalty of increasing γ_{ow} as surfactants are moved from interfacially active locations at the oil–water interface to the NP surface, and (3) the steric crowding at the NP surface at high grafting densities. The effect of NP-surfactant binding on γ_{ow} can be readily investigated. Plots of interfacial tension $versus$ surfactant coverage are given in Fig. 11 for varying D_e values.

For a constant number of surfactants an increase in D_e results in an increased interfacial tension. This, combined with the trajectories and the analysis of bound surfactant, confirms that surfactants which are bound onto the surface of the NP are not as effective in lowering the interfacial tension compared to those which are free. Furthermore, for the curves corresponding to $D_e = 39.7$ and 99.7 kcal mol^{-1}, increasing the nominal surfactant concentration does not significantly impact γ_{ow} because most of the surfactants are bound onto the NP surface. However, as seen in Fig. 11, after a critical threshold the oil–water interfacial
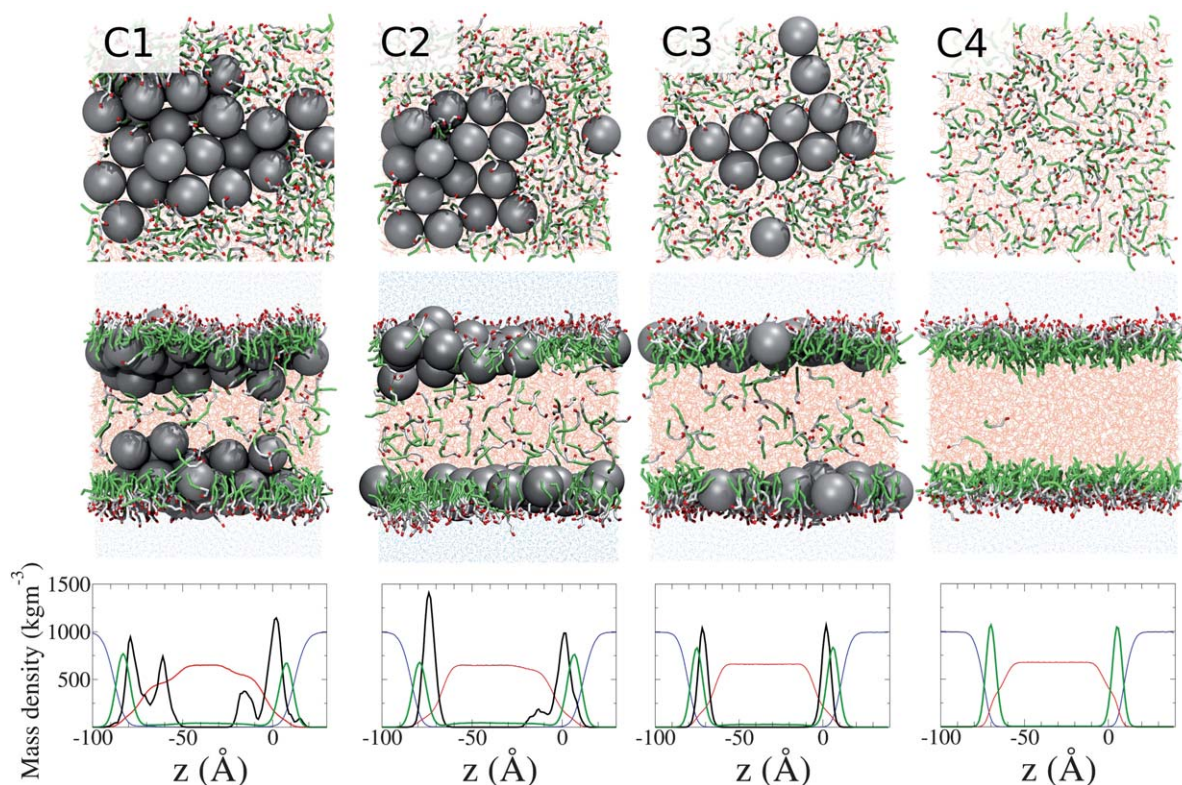

Fig. 8 Interfacial tension of the 125×125 Å^2 oil–water interface $versus$ the number of NPs localized at the interface. The up-triangles correspond to series (C) where free surfactant co-exists with NPs, while the down-triangles represent three systems (E4–E6) from series (E) where the surfactants are chemically bound to the surface of the NPs, which is described in the last section of the results and discussion. All points are at a constant nominal interfacial $C_{12}E_3$ coverage of 65.1 Å^2 per surfactant except for (E5) which is at 62.0 Å^2 per surfactant.

Fig. 9 Series (C). The top row of panels shows top-down views of representative configurations from simulations (C1), (C2), (C3), and (C4). The middle row shows side views while the bottom row shows the mass density profiles of the system components. The upper oil–water interface is at z ≈ 0. The same color scheme is used as in Fig. 1.
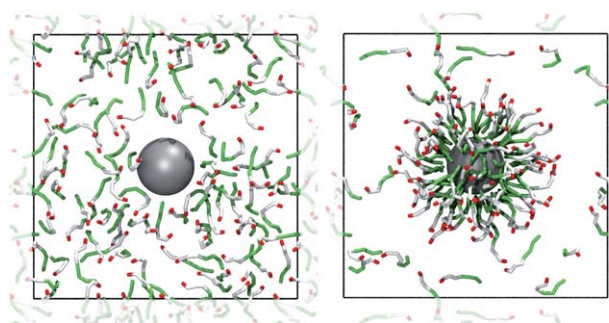

Fig. 10 Top view of the oil–water interface of system (D3). (Left) Free surfactant in the presence of a single NP. (Right) A Morse potential (of $D_e = 39.7$ kcal mol^{-1}) between the NP surface and the alkane termini of the surfactants drives chemical adsorption.

Fig. 11 The variation of interfacial tension with surfactant coverage for three dissociation energy (D_e) values for the NP–surfactant bond.

tension is lowered appreciably because the NP surface becomes saturated with surfactants beyond which the free surfactants are effective in lowering γ_{ow}.

3.6 Surfactant functionalized NPs

In this final section we study surfactant functionalizing the NP surface. Most synthetic routes encountered in the literature generate NP cores coated with surface functionalization. Non-ionic ligand functionalization of NPs is often used to provide a steric barrier to particle aggregation and sintering. In this section we focus on the 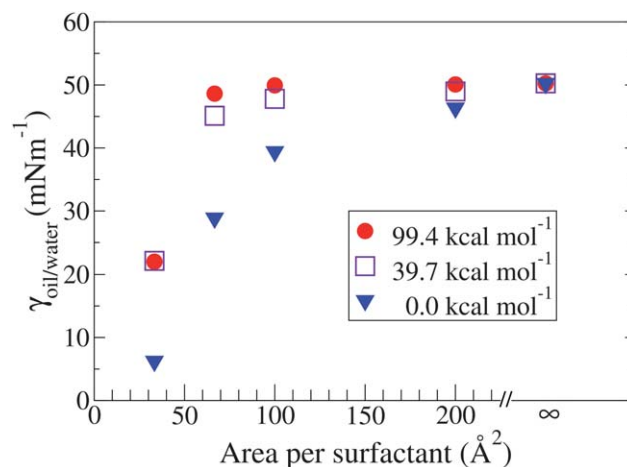effectivity of surfactant to lower the oil–water interfacial tension when irreversibly bound to a NP surface. Here the bond is modeled through the application of a harmonic potential (see methodology section) between the NP surface and the alkane termini of the surfactants.[29]

The choice of a harmonic potential allows for diffusion of the ligand over the surface of the NP. This model was chosen to allow maximum conformational freedom of the surfactants. Although the dynamics of the bond diffusion is artificial we are

only interested in equilibrium properties, and in real systems different mechanisms exist which result in equilibrium configurations where the ligands occupy low energy sites on the NP surface. For example, thiol ligands show remarkable lability when bound to either planar[41] or curved[16] gold surfaces. Another modeling choice for the ligand–NP bond would be to have static bonds. This would further attenuate the surfactant efficiency.

3.6.0.7 Series (E). In this series all the surfactants present in the simulation box are tethered to NPs. For comparison series (E) was designed such that (E1), (E2), (E3) has similar composition to (B2), (B3), (B4), while (E4), (E5), (E6) are similar to (C1), (C2), (C3). The surfactants are distributed evenly among the NPs. The tethering constrains mobility and hence prohibits surfactants from dissolving into the heptane phase. We can also expect this constraint to hamper the surfactant efficiency to lower γ_{ow}. Fig. 12 shows representative snapshots of two simulations carried out from series (E).

It is clear from the images that NP surface functionalization changes the particle aggregation properties. We have observed that binding of a small number (≤ 10) of $C_{12}E_3$ surfactants completely removes the free energy minimum seen in Fig. 5, transforming the free energy of dimerization to be completely repulsive. At low surface coverages of the NP (e.g. E5, Fig. 12) the surfactants retain adequate spatial freedom to adopt conformations that contribute to the lowering of γ_{ow}. However at high coverage densities (e.g. E3, Fig. 12) steric repulsion forces some surfactants to locations where their hydrophilic and hydrophobic blocks are not commensurate with the water and oil phases. Therefore at high coverage some surfactants are unlikely to contribute significantly towards lowering γ_{ow}.

The three sets of data shown in Fig. 13 are for surfactant only (series A), free surfactant in the presence of NPs (series B), and

Fig. 13 Surface tension as a function of apparent area per surfactant plotted for series (A), (B) and the corresponding simulations (E1–E3) of series (E). It is clear that the surfactants are less effective at lowering the oil–water interfacial tension when bound to NPs.

surfactants bound to NPs (series E). We previously noted some synergy for series (B). From Fig. 13 it is clear that the surfactants are not as effective in lowering the oil–water interfacial tension when bound to the NPs. There may be several reasons for this, including that the surfactants are forced into unfavorable positions with respect to the oil–water interface and inhomogenous surfactant interfacial coverage.

The interfacial tension values plotted in Fig. 8 compare series (C) with the analogous systems of series (E), where the concentration of surfactant is fixed and the number of NPs is varied. Since the number of surfactants is divided equally among the increasing number of NPs the surface density of surfactant gets progressively lower. Two opposing factors influence the interfacial tension: first the greater freedom of the surfactants at lower NP coverage which tends to decrease γ_{ow} and second the crowding of NPs at the interface which forces NPs (and their attached surfactants) into the oil phase.

4 Conclusion

In summary, we have carried out coarse grained molecular dynamics simulations of uncharged NPs and non-ionic surfactant at oil–water interfaces. We first studied the behavior of tri-(ethyleneglycol)-dodecyl ether surfactant and confirmed its effectivity and efficiency in lowering the oil–water interfacial tension. We also studied the behavior of uncharged NPs at an oil–water interface and found that although they localize at the interface they do not significantly alter the oil–water interfacial tension γ_{ow}. Collectively, we showed that surfactants and NPs exhibit synergistic behavior in lowering γ_{ow} at low surfactant concentration. However, we showed that with increased surfactant concentration the driving force for NP localization at the interface is diminished and factors other than the oil–water surface energy begin to dominate the free energy of the system. Therefore, at high concentration of surfactant the desorption of species into the oil phase is increased, which can be thought of as a competition for 'binding sites' at the oil–water interface.
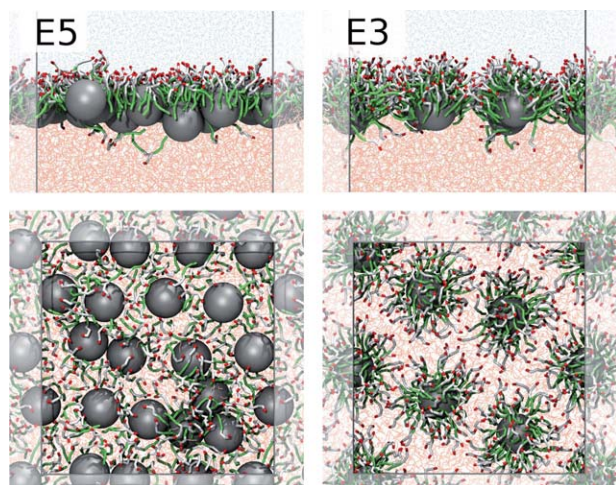

Fig. 12 Representative snapshots of simulations run in series (E). Here every surfactant is bound to a NP. At low $C_{12}E_3$ coverage on the surface of the NP (left: system E5) many surfactants are oriented suitably to lower the oil–water interfacial tension. At higher coverage densities (right: system E3), steric repulsion forces some surfactants into unfavorable conformations. The functionalized NPs are seen to adopt very different packing structures from their unfunctionalized counterparts (see Fig. 6, 9).
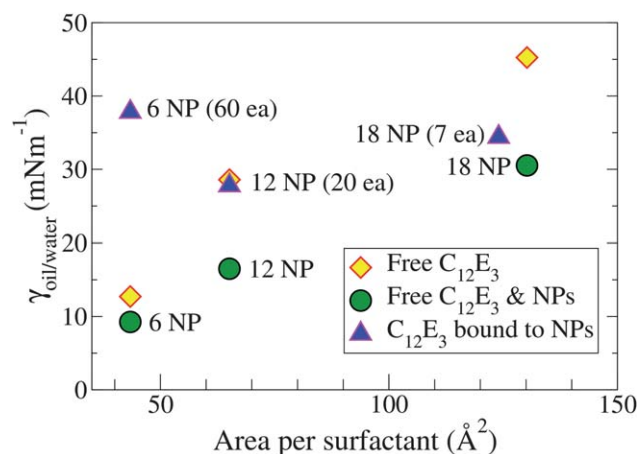
The influence of surfactant chemisorption to the NP surface was studied by assigning a Morse potential between the two components. It was found that the spatial confinement of surfactants upon adsorption onto the NP surface lowered their efficiency in stabilizing the oil–water interface. Furthermore, it was found that chemisorbed surfactants are effective in imposing a steric barrier towards particle–particle aggregation.

Throughout this article we have limited ourselves to the study of uncharged species and hence we have examined the role of dispersive interactions on the behavior of NPs and surfactants in co-existence. This is important because these interactions are ubiquitous in all chemical systems. However, it must be acknowledged that we are still merely scratching the surface of these complex systems. Further investigations may involve studying the influence of the particle-solvent interaction strength on the behavior of the system, the use of spread surfactants (Langmuir monolayer) as opposed to an adsorbed surfactant (Gibbs monolayer), and the introduction of charged species.

References

1 M. Deleu and M. Paquot, *C. R. Chim.*, 2004, **7**, 641–646.
2 V. M. Dembitsky, *Lipids*, 2004, **39**, 933–953.
3 M. J. Rosen, *Surfactants and Interfacial Phenomena*, John Wiley & Sons, Incorporated, 2004.
4 *Colloidal Particles at Liquid Interfaces*, ed. B. P. Binks, Cambridge University Press, 2006.
5 S. Kinge, M. Creg-Calama and D. N. Reinhoudt, *ChemPhysChem*, 2008, **9**, 20–42.
6 D. Wang, H. Duan and H. Mohwald, *Soft Matter*, 2005, **1**, 412–416.
7 A. D. Dinsmore, M. F. Hsu, M. G. Nikolaides, M. Marquez, A. R. Bausch and D. A. Weitz, *Science*, 2002, **298**, 1006–1011.
8 A. Boker, J. He, T. Emrick and T. P. Russell, *Soft Matter*, 2007, **3**, 1231–1248.
9 M. Luo, Y. Song and L. L. Dai, *Mol. Simul.*, 2009, **35**, 773–784.
10 W. Shinoda, R. DeVane and M. L. Klein, *Soft Matter*, 2008, **4**, 2454–2462.
11 F. Schmid, *Macromol. Rapid Commun.*, 2009, **30**, 741–751.
12 R. J. B. Kalescky, W. Shinoda, P. B. Moore and S. O. Nielsen, *Langmuir*, 2009, **25**, 1352–1359.
13 H. C. Hamaker, *Physica*, 1937, **4**, 1058–1072.
14 A. D. MacKerell, D. Bashford, M. Bellott, R. L. Dunbrack, J. D. Evanseck, M. J. Field, S. Fischer, J. Gao, H. Guo, S. Ha, D. Joseph-McCarthy, L. Kuchnir, K. Kuczera, F. T. K. Lau, C. Mattos, S. Michnick, T. Ngo, D. T. Nguyen, B. Prodhom, W. E. Reiher, B. Roux, M. Schlenkrich, J. C. Smith, R. Stote, J. Straub, M. Watanabe, J. Wiorkiewicz-Kuczera, D. Yin and M. Karplus, *J. Phys. Chem. B*, 1998, **102**, 3586–3616.
15 C. Chiu, P. B. Moore, W. Shinoda and S. O. Nielsen, *J. Chem. Phys.*, 2009, **131**, 244706.
16 A. M. Jackson, J. W. Myerson and F. Stellacci, *Nat. Mater.*, 2004, **3**, 330–336.
17 W. Shinoda and M. Mikami, *J. Comput. Chem.*, 2003, **24**, 920–930.
18 W. G. Hoover, *Phys. Rev. A: At., Mol., Opt. Phys.*, 1985, **31**, 1695–1697.
19 H. C. Andersen, *J. Chem. Phys.*, 1980, **72**, 2384–2393.
20 M. E. Tuckerman, B. J. Berne and G. J. Martyna, *J. Chem. Phys.*, 1991, **94**, 6811–6815.
21 Y. Zhang, S. E. Feller, B. R. Brooks and R. W. Pastor, *J. Chem. Phys.*, 1995, **103**, 10252–10266.
22 W. Rawicz, K. Olbrich, T. McIntosh, D. Needham and E. Evans, *Biophys. J.*, 2000, **79**, 328–339.
23 W. Russel, D. Saville and W. Schowalter, *Colloidal Dispersions*, Cambridge University Press, 1989.
24 T. N. Hunter, R. J. Pugh, G. V. Franks and G. J. Jameson, *Adv. Colloid Interface Sci.*, 2008, **137**, 57–81.
25 F. Ravera, M. Ferrari, L. Liggieri, G. Loglio, E. Santini and A. Zanobini, *Colloids Surf., A*, 2008, **323**, 99–108.
26 R. A. Sperling and W. J. Parak, *Philos. Trans. R. Soc. London, Ser. A*, 2010, **368**, 1333–1383.
27 R. Nagarajan and E. Ruckenstein, *Langmuir*, 1991, **7**, 2934–2965.
28 P. Pieranski, *Phys. Rev. Lett.*, 1980, **45**, 569–573.
29 R. J. K. U. Ranatunga, R. J. B. Kalescky, C. Chiu and S. O. Nielsen, *J. Phys. Chem. C*, 2010, **114**, 12151–12157.
30 D. Chandler, *Introduction to Modern Statistical Mechanics*, Oxford University Press, 1987.
31 J. C. Berg, *An Introduction to Interfaces & Colloids: the Bridge to Nanoscience*, World Scientific Publishing, 2010.
32 T. Okubo, *J. Colloid Interface Sci.*, 1995, **171**, 55–62.
33 L. Dong and D. T. Johnson, *J. Dispersion Sci. Technol.*, 2004, **25**, 575–583.
34 B. P. Binks, *Curr. Opin. Colloid Interface Sci.*, 2002, **7**, 21–41.
35 Y. Lin, A. Boker, H. Skaff, D. Cookson, A. D. Dinsmore, T. Emrick and T. P. Russell, *Langmuir*, 2005, **21**, 191–194.
36 D. E. Tambe and M. M. Sharma, *J. Colloid Interface Sci.*, 1993, **157**, 244–253.
37 W. Wang, Z. Zhou, K. Nandakumar, Z. Xu and J. H. Masliyah, *J. Colloid Interface Sci.*, 2004, **274**, 625–630.
38 K.-L. Gosa and V. Uricanu, *Colloids Surf., A*, 2002, **197**, 257–269.
39 B. R. Midmore, *Colloids Surf., A*, 1998, **145**, 133–143.
40 B. P. Binks, A. Desforges and D. G. Duff, *Langmuir*, 2007, **23**, 1098–1106.
41 C. Vericat, M. E. Vela and R. C. Salvarezza, *Phys. Chem. Chem. Phys.*, 2005, **7**, 3258–3268.